P2.12   THE EFFECT OF SHEAR DISCONTINUITIES AND CRITICAL LEVELS
ON OROGRAPHIC GRAVITY WAVE DRAG

Miguel A. C. Teixeira[1]*, Pedro M. A. Miranda[1] and José L. Argaín[2]
[1]CGUL, IDL, University of Lisbon, Lisbon, Portugal
[2]Department of Physics, University of Algarve, Faro, Portugal

1. INTRODUCTION

In idealized studies of mountain waves, particularly those addressing critical levels, wind profiles that vary linearly are often assumed as a crude approximation to real wind profiles with shear (e.g. Booker and Bretherton 1967). That is the case also in the study of Grubišić and Smolarkiewicz (1997), where the surface gravity wave drag is calculated. In reality, wind profiles that vary linearly near the surface must be bounded aloft, so the shear must change at some height. Shear variations are likely to affect the drag, through multiple reflections of the wave energy between the surface and the levels where they occur (Teixeira et al. 2005). Most studies have considered relatively weak shear (i.e. flow at relatively high Richardson number, Ri), but that is not the case of Grubišić and Smolarkiewicz (1997), where the drag variation is studied for Ri down to 1/4. For this range of Ri, both shear discontinuities and critical levels are likely to strongly affect the surface drag. At low Ri, the effect of critical levels can no longer be treated as total wave absorption.

In the present study, the effects of shear discontinuities and critical levels are addressed using linear theory and numerical simulations for relatively low Ri. We consider inviscid, non-rotating, hydrostatic and uniformly stratified atmospheric flow over 2D and 3D mesoscale mountains. In order to isolate the effects under consideration, very simple idealized wind profiles are adopted: the wind velocity is assumed to vary linearly up to a certain level, and to be constant above it.

Shear discontinuities may either enhance or reduce the surface drag, depending on whether they lead to constructive or destructive interference between upward and downward propagating waves. The surface drag is also highly sensitive to the existence (or not) of critical levels between the surface and the shear discontinuity. The cases of unidirectional shear and directional shear flow must be distinguished. While for unidirectional shear, all wavenumbers in the mountain waves' spectrum either have or do not have a critical level, for directional shear some wavenumbers have critical levels whereas others do not. Cases with unidirectional shear are treated here using a 2D ridge, whereas cases with directional shear require 3D orography. In the latter situation, a circular mountain is adopted for simplicity.

Apart from their intrinsic fundamental interest, the results reported in this study are also relevant for the improvement of drag parameterization schemes, since

Corresponding author address: Miguel A. C. Teixeira, Centro de Geofísica da Universidade de Lisboa, Edifício C8, Campo Grande, 1749-016 Lisbon, Portugal; e-mail: mateixeira@fc.ul.pt

these schemes generally do not take vertical wind shear into account,

2. THEORETICAL MODEL

We depart from the hydrostatic version of the Taylor-Goldstein equation,

$$\hat{w}'' + \frac{N^2(k^2 + l^2)}{(Uk + Vl)^2}\hat{w} = 0 \, , \qquad (1)$$

where the wind profile curvature term has been neglected, since only piecewise-linear wind profiles will be considered. $\hat{w}$ is the Fourier transform of the vertical velocity perturbation, N is the Brunt-Väisälä frequency of the background flow (assumed constant), $(U(z),V(z))$ is the background wind velocity, (k,l) is the horizontal wavenumber of the internal gravity waves, and the primes denote differentiation with respect to height, z.

The background wind profile is assumed to have the form:

$$U = U_0 + \alpha z, \ V = V_0 + \beta z \quad \text{if} \quad z < z_1 \, ,$$

$$U = U_1 = U_0 + \alpha z_1, \ V = V_1 = V_0 + \beta z_1 \quad \text{if} \quad z > z_1 \, , \quad (2)$$

where U_0, V_0, α and β are constants. So the wind varies linearly below the height z_1, and is constant above that height. For this wind profile, the solution to (1) in the lower layer is

$$\hat{w} = \gamma \left(1 + \frac{\alpha k + \beta l}{U_0 k + V_0 l} z\right)^{\frac{1}{2} - i\mu s} + \delta \left(1 + \frac{\alpha k + \beta l}{U_0 k + V_0 l} z\right)^{\frac{1}{2} + i\mu s} , \quad (3)$$

where γ and δ are constants, $s = \text{sign}(\alpha k + \beta l)$ and

$$\mu = \left[\frac{N^2(k^2 + l^2)}{(\alpha k + \beta l)^2} - \frac{1}{4}\right]^{\frac{1}{2}} . \qquad (4)$$

In the upper layer, on the other hand, the solution is:

$$\hat{w} = \varepsilon \exp\left[i \frac{N(k^2 + l^2)^{1/2}}{U_1 k + V_1 l} z\right], \qquad (5)$$

where ε is a constant. In (3), the two terms correspond to waves whose energy propagates upward and downward, while in (5) only upward propagating waves are considered, since the source of the waves is at the surface. In order to determine the constants γ, δ and ε, it is necessary to note that both $\hat{w}$ and the Fourier transform of the pressure perturbation associated with the waves,

$$\hat{p} = i \frac{\rho_0}{k^2 + l^2}\left[(U'k + V'l)\hat{w} - (Uk + Vl)\hat{w}'\right], \qquad (6)$$

(where ρ_0 is a constant reference density) must be continuous at $z = z_1$. Additionally, the boundary condition at the surface is

$$\hat{w}(z = 0) = i(U_0 k + V_0 l)\hat{h} \, , \qquad (7)$$

where $\hat{h}$ is the Fourier transform of the terrain elevation. These conditions totally define the solution to the present mountain wave problem.

The drag produced by mountain waves is given by

$$(D_x, D_y) = 4\pi^2 i \int_{-\infty}^{+\infty}\int_{-\infty}^{+\infty} (k,l)\hat{p}^*(z=0)\hat{h}\,dk\,dl \qquad (8)$$

for a 3D mountain. For a 2D mountain, all the previous equations (apart from (8)) remain valid as long as it is noted that in this case $l=0$, $V_0=0$ and $\beta=0$. Then the drag per unit length in the spanwise direction is

$$D = 2\pi i \int_{-\infty}^{+\infty} k\hat{p}^*(z=0)\hat{h}\,dk \;, \qquad (9)$$

where now all Fourier transforms must be understood as 1D instead of 2D.

In order to address the effects of shear discontinuities and critical levels only, the values of the drag given by (8) and (9) will be normalized by the corresponding values due to a constant wind equal to the surface wind.

3. RESULTS

The variation of the normalized drag with Ri will be studied first for unidirectional shear flow over a 2D ridge. This situation is the simplest to interpret. Then, results will be presented for directional shear flow over a circular mountain. A circular mountain is chosen because it possesses an isotropic spectrum that is particularly convenient to isolate the effect of critical levels. Additionally, the 2D and circular geometry have the advantage of making the normalized drag independent of the detailed shape of the orography. This is only valid for hydrostatic and non-rotating flow, such as considered here. All wind profiles used are of the type given by (2).

3.1 *Unidirectional shear flow over a 2D ridge*

We first consider the wind profile (2) with $V_0=\beta=0$ and flow over a 2D ridge aligned in the y direction ($l=0$). If $U_0>0$, two situations are possible: forward shear ($\alpha>0$), or backward shear ($\alpha<0$). In the case of backward shear, it will be assumed that a critical level exists, i.e. $U=0$ at some height below z_1. (the case of backward shear without a critical level is identical, in terms of drag behavior, to the case of forward shear).

Figure 1 shows the normalized drag as a function of Ri^{-1} for different values of the ratio of the wind speed at z_1 and at $z=0$, $|U_1/U_0|$. In Fig. 1a the case of forward shear is displayed, whereas in Fig. 1b, the shear is backward. The lower and upper solid lines correspond, respectively, to the exact linear drag (Smith 1986)

$$\frac{D}{D_0} = \left(1 - \frac{1}{4Ri}\right)^{\frac{1}{2}}, \qquad (10)$$

and to the drag calculated using a WKB approximation (Teixeira and Miranda 2004) for a shear that extends indefinitely:
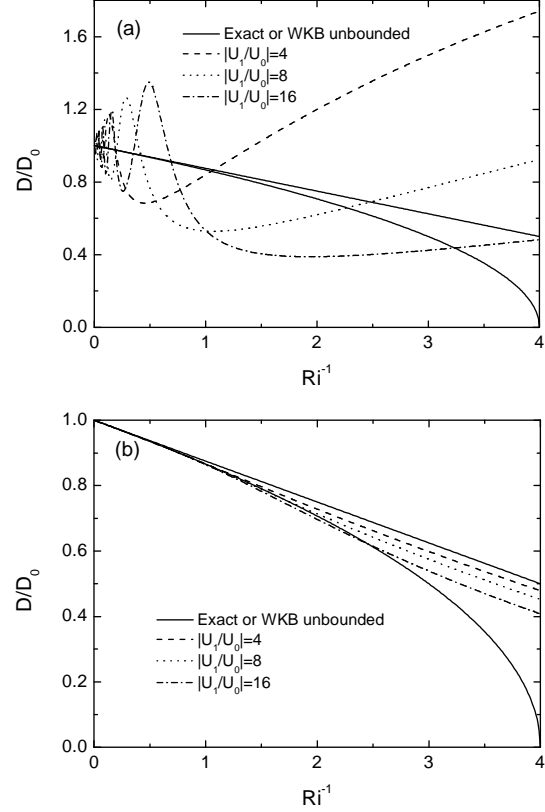

Figure 1. Normalized drag as a function of Ri^{-1} for unidirectional flow over a 2D ridge, for various values of $|U_1/U_0|$. (a) Forward shear, (b) backward shear.

$$\frac{D}{D_0} = 1 - \frac{1}{8Ri} \;. \qquad (11)$$

It can be seen that, in the case of forward shear, the behavior of the drag differs markedly from that predicted for an infinite shear layer. The drag oscillates, attaining maxima at low Ri that can be considerably larger than predicted by previous models. By contrast, for backward shear, the drag has no oscillations and stays much closer to the predictions of both exact theory and WKB theory for an infinite shear layer.

This behavior is explained by Fig. 2, where the reflection coefficient, defined as

$$R = \left|\frac{\gamma}{\delta}\right|, \qquad (12)$$

is presented as a function of Ri^{-1}. For forward shear, R decreases gradually to zero as Ri^{-1} decreases from 4 to 0. This is due to the smoothing of the shear discontinuity at z_1. On the other hand, for backward shear, R decays much faster. This is due to wave absorption at the critical level below z_1. Hence, for forward shear, resonance is produced by upward and downward propagating waves in the layer below z_1. This leads to the observed drag oscillations. For backward shear, these oscillations are largely precluded. At Ri=0.5, for example, almost all of the wave energy is absorbed, which manifestly is not the case for forward shear.
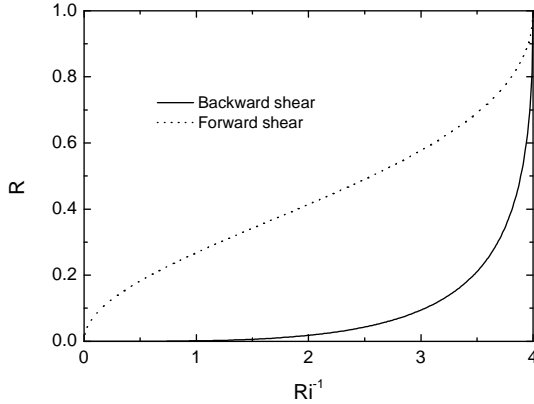
Figure 2. Reflection coefficient as a function of Ri^{-1}.

The foregoing results are linear. We also carried out numerical simulations to see in what way these results changed for more realistic mountain heights (see Teixeira et al. 2008 for details). A dimensionless mountain height of $Nh_0/U_0=0.5$ was considered (where h_0 is the dimensional height). This corresponds to relatively weak nonlinearity. Figure 3 shows theoretical results (lines) and numerical results (symbols) for one particular value of $|U_1/U_0|=4$. The nonlinear results are denoted by the open squares. It can be seen that, in
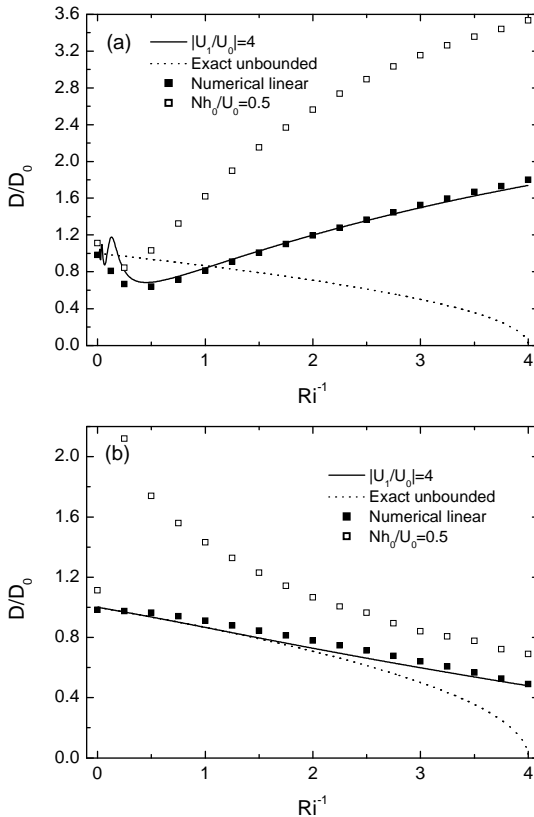

Figure 3. Normalized drag as a function of Ri^{-1} for $|U_1/U_0|=4$ in linear and nonlinear conditions. (a) Forward shear, (b) backward shear.

nonlinear conditions, the drag is considerably amplified, but in different ways for forward and backward shear. For forward shear, the drag is amplified especially at low Ri, while for backward shear, it is amplified particularly at high Ri (but very little at $Ri^{-1}=0$). This leads to an apparent singularity in the drag variation at high Ri, which probably can be attributed to nonlinear critical level dynamics (Teixeira et al. 2008).

### 3.2 *Directional shear flow over a circular mountain*

Unidirectional flow over a 3D mountain is affected essentially in the same way as unidirectional flow over a 2D mountain, with the difference that the waves are now dispersive. Therefore, the drag behaves essentially as in Fig. 3 (with a somewhat smaller degree of amplification in the case of Fig. 3a).

The situation is different for flows with directional shear, since in that case a critical level is not simply a level where the background wind velocity vanishes, but rather a level where

$$Uk + Vl = 0 . \qquad (13)$$

As is clear from (13), critical levels are located at different heights for each wavenumber, which means that, as the background wind rotates, there is a continuous distribution of these levels. Then, instead of having all or none of the wave spectrum filtered by a critical level, there are parts of the wave spectrum that are filtered and others that are not. This leads to a drag behavior that is intermediate between that of Fig. 1a or Fig. 3a and that of Fig. 1b or Fig. 3b.

First we will consider a background wind profile that, below z_1, is similar to that adopted by Shutts and Gadian (1999). This corresponds to taking $V_0=0$, $\alpha=0$, $U_0>0$, $\beta>0$ in (2). Figure 4 shows the drag variation with Ri^{-1} for this wind profile for various values of $|U_1/U_0|$. Symbols are as in Fig. 1. Both components of the drag have oscillations with Ri, but do not reach as high values as in Fig. 1. Interestingly, due to its oscillations, the y component of the drag becomes negative, for example at Ri=0.5. This means this component of the drag opposes the corresponding wind component, i.e.,
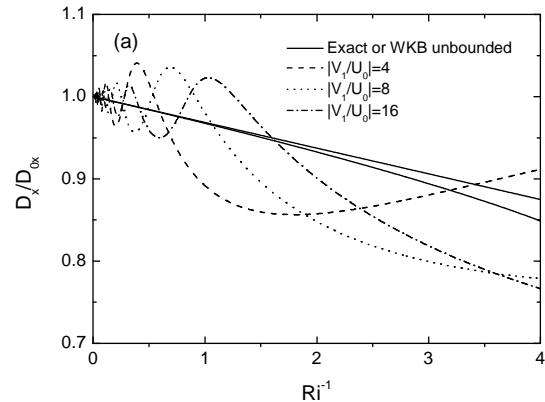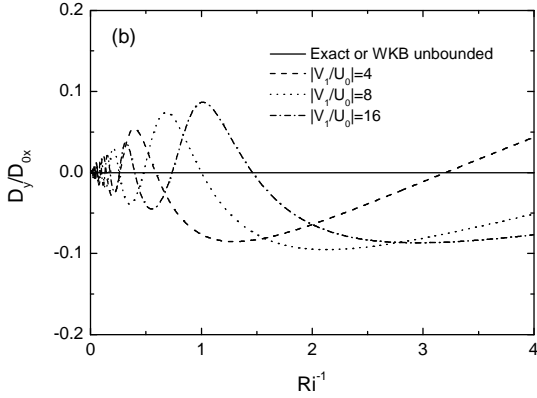
Figure 4. Normalized drag as a function of Ri^{-1} for the wind profile of Shutts and Gadian (1999) over a circular mountain for various values of $|U_1/U_0|$. (a) x component, (b) y component.

the mountain is accelerating the wind.

The reason for the lower amplitude of the drag oscillations is the following. For the assumed wind profile, the angle spanned by the wind velocity is at most $\pi/2$. Since all wavenumbers that are perpendicular
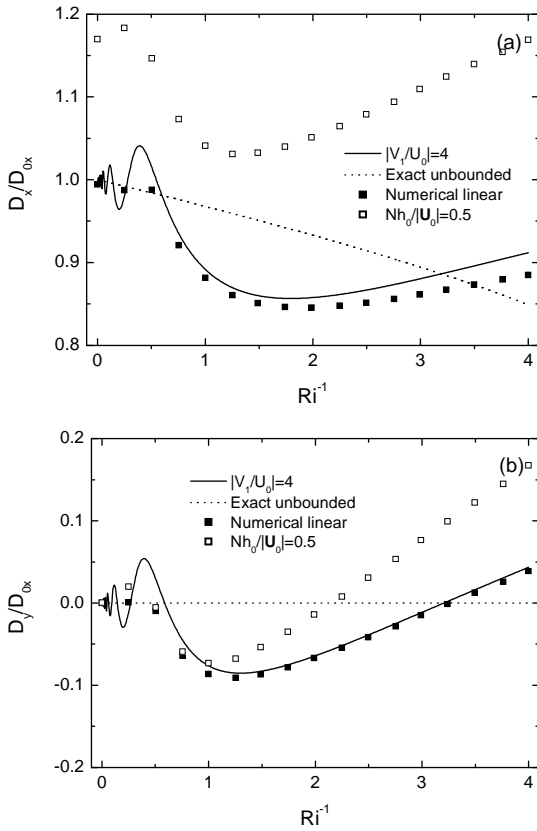
to the wind are filtered by critical levels, this means that critical levels exist for at most a range of wavenumber angles of π, or half of the total spectrum. This leads to partial filtering of the mountain wave spectrum, which, while retaining the drag oscillations, somewhat reduces their amplitude.

In weakly nonlinear conditions ($Nh_0/U_0=0.5$) the drag is somewhat amplified, but not so much as in Fig. 3. This is due, on the one hand to the wave dispersion inherent to any 3D flow, and on the other to the partial wave filtering mentioned above.

Finally, we consider a wind profile that, below z_1, is similar one of those used by Teixeira et al. (2004). This corresponds to setting $V_0=U_0>0$, $\beta=0$ and $\alpha<0$ in (2). This wind profile has the property of spanning, at most, an angle of $3\pi/4$, which means that the waves filtered from the complete spectrum span an angular range of at most $3\pi/2$, or 3/4 of the possible maximum range. This situation therefore corresponds to considerably more complete wave filtering.

Figure 6 shows the drag as a function of Ri^{-1} for the same values of $|U_1/U_0|$ as employed in Figs. 1 and 4. The drag now oscillates much less than in either Fig. 1 or Fig. 4, especially the x component. This is due to the fact that only abut 1/4 of the wave spectrum reaches the shear discontinuity at z_1 without passing through a

Figure 5. Normalized drag as a function of Ri^{-1} for $|U_1/U_0|=4$ in linear and nonlinear conditions. (a) x component, (b) y component.
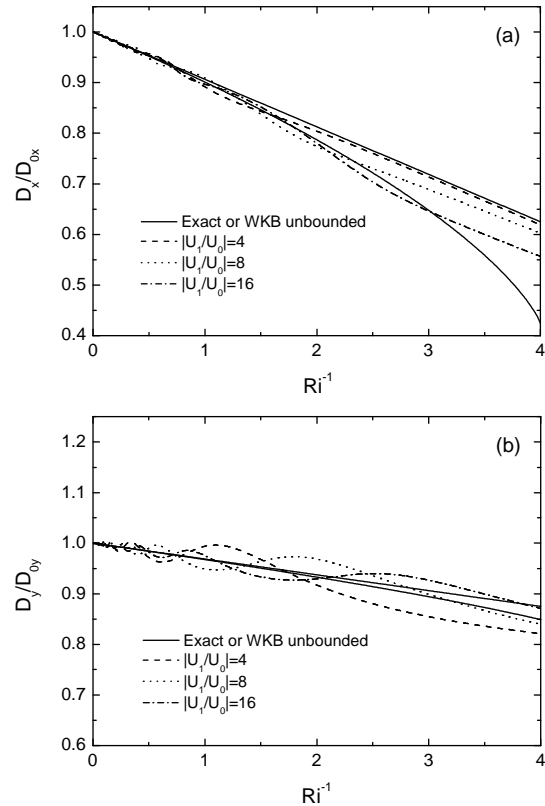

Figure 6. Normalized drag as a function of Ri^{-1} for the wind profile of Teixeira et al. (2004) over a circular mountain for various values of $|U_1/U_0|$.(a) x component, (b) y component.
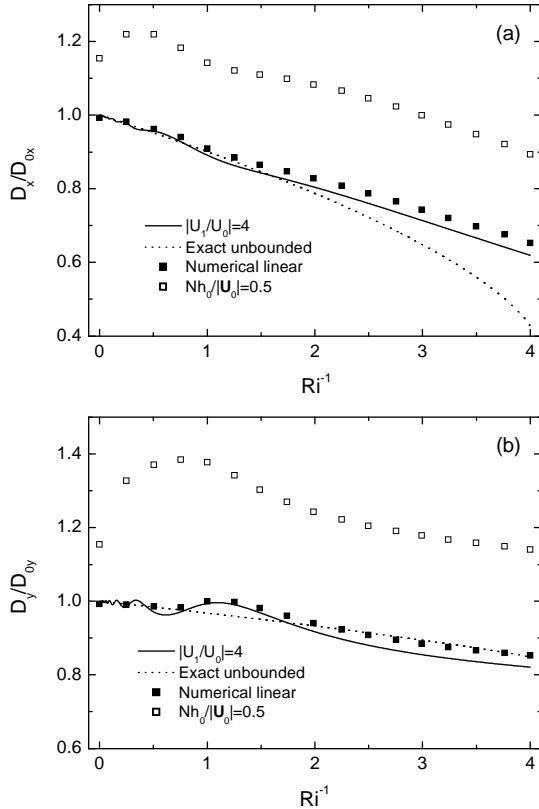
Figure 7. Normalized drag as a function of Ri^{-1} for $|U_1/U_0|=4$ in linear and nonlinear conditions. (a) x component, (b) y component.

critical level. This relatively small part of the spectrum is responsible for the remaining drag oscillations, particularly visible in Fig. 6b. Otherwise, the drag variation is relatively close to the predictions valid for an infinite shear layer, both derived exactly or using a WKB approximation.

In nonlinear conditions, again for $Nh_0/U_0=0.5$, both components of the drag are considerably amplified for all non-zero values of Ri^{-1}, but less than in Fig. 3. An apparent singularity at high Ri, where the drag changes from its relatively modest increase at $Ri^{-1}=0$ to a larger increase at $Ri^{-1}\neq0$ is also seen in this case, but the transition is more smoothed. This is consistent with the fact that now only a part of the spectrum (that which passes through critical levels) is affected by this process.

4. CONCLUDING REMARKS

It was seen that, in an atmosphere where the wind varies linearly below a certain height and becomes constant aloft, the behavior of mountain wave drag is considerably more complicated than in an (idealized) atmosphere where the shear extends indefinitely. For unidirectional shear flow, differences only depend on whether there is a (total) critical level or not. When there is no critical level (e.g. for forward shear), the drag variation as a function of Ri is characterized by strong

oscillations, and bears no resemblance to the drag for a similar shear that extends indefinitely. This is caused by resonance associated with interference between waves whose energy propagates upward and downward beneath the shear discontinuity. For backward shear with a critical level, the drag oscillations are nearly absent, and the drag stays close to results for an infinite shear layer, either exact or derived using a WKB approximation. This is due to the filtering, or absorbing, effect of critical levels.

For directional shear flows over a circular mountain, it was seen that the greater the amount of critical levels that the waves encounter, the closer the drag is to its predicted value for a shear of unlimited extent. The dependence of the drag on the fraction of wavenumbers filtered by critical levels creates an asymmetry between flows with positive and negative shear. This asymmetry is not predicted by linear theory for a shear extending indefinitely in hydrostatic conditions. Since many theoretical studies on gravity waves assume constant-shear flows, the present study highlights the importance of taking into account the shear discontinuities, or shear variations, that always exist in practice.

Nonlinear effects are found to considerably amplify the drag, but many qualitative features of the linear drag behavior remain. However, differences between linear and nonlinear results are substantially enhanced by the existence of shear, being much more pronounced than for a constant wind.

5. REFERENCES

Booker, J. R. and Bretherton, F. P., 1967: The critical layer for internal gravity waves in a shear flow. *J. Fluid Mech.*, **27**, 513-539.

Grubišić, V. and Smolarkiewicz, P. K., 1997: The effect of critical levels on 3D orographic flows: linear regime. *J. Atmos. Sci.*, **54**, 1943-1960.

Shutts, G. J. and Gadian, A., 1999: Numerical simulations of orographic gravity waves in flows which back with height. *Quart. J. Roy. Meteor. Soc.*, **125**, 2743-2765.

Smith, R. B., 1986: Further development of a theory of lee cyclogenesis. *J. Atmos. Sci.*, **43**, 1582-1602.

Teixeira, M. A. C. and Miranda, P. M. A., 2004: The effect of wind shear and curvature on the gravity wave drag produced by a ridge. *J. Atmos. Sci.*, **61**, 2638-2643.

Teixeira, M. A. C., Miranda, P. M. A. and Argaín, J. L., 2005: Resonant gravity-wave drag enhancement in linear stratified flow over mountains. *Quart. J. Roy. Meteor. Soc.*, **131**, 1795-1814.

Teixeira, M. A. C., Miranda, P. M. A. and Argaín, J. L., 2008: Mountain waves in two-layer sheared flows: critical-level effects, wave reflection and drag enhancement. *J. Atmos. Sci.*, **65**, 1912-1926.

Teixeira, M. A. C., Miranda, P. M. A. and Valente, M. A. 2004: An analytical model of mountain wave drag for wind profiles with shear and curvature. *J. Atmos. Sci.*, **61**, 1040-1054.